Hindawi
Shock and Vibration
Volume 2022, Article ID 6875718, 17 pages
https://doi.org/10.1155/2022/6875718

Research Article

An Analytical, Numerical, and Experimental Investigation on Transverse Vibrations of a Finite Locally Resonant Beam

Peng Guo and Qizheng Zhou

College of Weaponry Engineering, Naval University of Engineering, Wuhan 430033, China

Correspondence should be addressed to Qizheng Zhou; qizheng509@163.com

Received 29 March 2022; Accepted 20 May 2022; Published 13 June 2022

Academic Editor: Sami El-Borgi

An analytical, numerical, and experimental investigation on the transverse vibrations of a finite beam with periodically arrayed beam-like resonators was carried out. A continuous-discrete model of the finite locally resonant beam was established by employing the "mass-spring- mass" subsystem. The analytical solution of the coupling vibration equations was derived based on the modal superposition method, and the analytical expression of average velocity response and vibration transmissibility were given. Then, the minimum periodic number of different units which could result in a bandgap was determined. Finally, the bandgap of a finite locally resonant beam was confirmed by a vibration experiment on a simply supported beam with twelve uniformly distributed beam-like resonators. The numerical and experimental results show that finite locally resonant beams have low-frequency bandgaps like infinite locally resonant beams, and the bandgap position is close to the resonance frequency of resonators. In addition, for a beam with a different type of locally resonant units, the minimum number of units that can generate the bandgap is nearly the same. Within considered frequency ranges, the experimental results are consistent with the theoretical results, meaning that the transverse vibration in locally resonant beams could be substantially attenuated. The conclusions may be supported to the application of locally resonant theory to control low-frequency vibration and radiation noise.

1. Introduction

Structures with periodically attached resonators which can manipulate the elastic wave propagation have been applied to the vibration and noise attenuation or isolation in mechanical and structural engineering. Beams as typical structural elements in practical engineering, low-frequency vibration control methods of beams have always been a relevant issue. Due to the "effective" negative mass density [1] and negative moduli [2] in certain frequency ranges, beams with periodically attached resonators (locally resonant beams) can prevent elastic waves completely, this overcomes the limitation of wavelength to control lower-frequency vibration by subwavelength structures. This is different from traditional bandgap generation mechanisms such as the Bragg scattering mechanism. However, there are still challenges in applying the locally resonant mechanism to control low-frequency vibration and radiation noise of beams.

Since the concept of a locally resonant mechanism was proposed [3], investigations of such structures have received much attention for their promise of physical properties and potential applications. A locally resonant beam is usually modelled as a continuous-discrete system, where a continuous beam is coupled with discrete subsystems. The discrete subsystems are used to describe the vibration of resonators which are regarded as single or multidegree- of-freedom "spring-damping-mass" systems. The locally resonant beam is usually considered to be an infinite system, and many solutions have been employed to calculate the vibration transmission properties of locally resonant beams, such as the transfer matrix method [4, 5], the plane wave expansion method [6–9], the finite element method [10, 11], the generalized function method [12], and the direct integration and complex modal analysis approach [13]. These methods considered a single unit of locally resonant structure with the Floquet–Bloch periodic condition, which

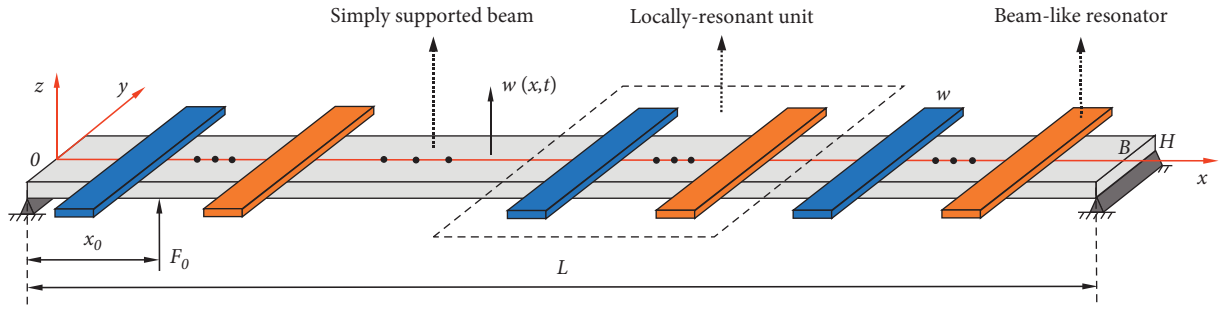

Figure 1: A dynamic model of the finite locally resonant beam.

was mainly suitable for the infinite periodic structure. However, the bandgap properties of finite locally resonant beams are more important in practical engineering applications. Recently, the boundary conditions were proved to be an important factor on the bandgap characteristics of these beams. Sangiuliano et al. [14] investigated the influence of boundary conditions on the bandgap of the finite locally resonant beam and found that the boundary conditions could weaken the level of vibration attenuation.

The bandgap of locally resonant beams is closely related to the parameters of resonators; many studies are devoted to bandgap adjustments such as broadening the bandgap or generating multiple bandgaps. To broaden the frequency range of the bandgap in a locally resonant beam, the application of continuous vibration absorbers [15] and distributed dynamic absorbers by Chen and Wu [16] has been proposed. Wang et al. [17] considered two types of resonators attached to a free Euler–Bernoulli beam and investigated the effects of the separation distance of resonators on the further widening of the bandgaps. By using multiple resonators, Zhou et al. [18] investigated the multilow-frequency bandgaps in beams by adding more resonators with different resonance frequencies surrounding the target frequency. Claeys et al. [19] proposed a novel lightweight solution of locally resonant subsystems, which were designed as cantilever beams with additional mass at the end and investigated the efficiency of the locally resonant structure numerically and experimentally. The vibration absorber is a common realization form of the resonator, and the nonlinear vibration absorber has a good research prospect in bandgap expansion. Habib et al. [20] introduced a nonlinear vibration absorber for mitigating the nonlinear resonance of a mechanical system and developed a nonlinear generalization of Den Hartog's equal-peak method which can provide a reference for the design of vibration absorbers. Casalotti and Lacarbonara [21] investigated the response of the nonlinear vibration absorber to harmonic excitations by the asymptotic approach and explored transfers of energy from the structure to the absorber which achieved optimal vibration amplitude reduction. In another work, Casalotti et al. [22] applied nonlinear absorbers to the vibration reduction design of the hinged-hinged beam, then studied and optimized the multimode vibration absorption capability of the metamaterial beam with an array of embedded nonlinear absorbers.

In this paper, the bandgap characteristics of the locally resonant beam with finite boundary are investigated, and the locally resonant bandgap is calculated by the modal superposition method and the harmonic balance method, which is different from the calculation method for structure with infinite boundary. The coupling effect between the additional resonators and the beam can weaken the propagation of vibration waves in the structure, which is the essence of the vibration reduction effect of the locally resonant bandgap. In the study of the finite locally resonant beam, the number of resonators is an important factor affecting its bandgap characteristics. Hence, the effect of the number and parameters of the additional resonators on the bandgap is studied, and the minimum number of units that can generate the bandgap is determined in this paper.

This paper is organized as follows: following this introduction, we propose a locally resonant beam with periodically attached beam-like resonators and the equivalent simplified model and derive the analytical solution of the coupled vibration with the modal superposition method in Section 2. Section 3 includes the effects of the structural parameters of beam-like resonators and the type and numbers of locally resonant units on the vibration attenuation performance of the finite locally resonant beam. In Section 4, we describe the design and fabrication of a locally resonant beam experimental sample and compare the experimental results with the theoretical and numerical solutions. Finally, the findings are summarized in Section 5.

2. Model and Formulations

2.1. Model and Simplification. The finite locally resonant beam considered here consists of a simply supported aluminum beam and periodic arrays of several beam-like resonators, in which the "periodic arrays" of beam-like resonators refer to M locally resonant units and each unit contains N beam-like resonators so that the total number of resonators can be defined as MN. A dynamic model of a finite locally resonant beam is shown in Figure 1. The length and cross-sectional of the beam are L and A, respectively. The dimension of the beam-like resonator is $2l \times w \times t$, where l_s is the rigid support length of the beam-like resonator, as denoted in Figure 2(a). The simply supported beam vibrated under a harmonic point force $F(t) = F_0 \sin \omega t$ at the coordinate of x_0.

Assuming each beam-like resonator is connected to the host beam by a lumped point when the first resonant frequency is of a smaller order than the other resonant

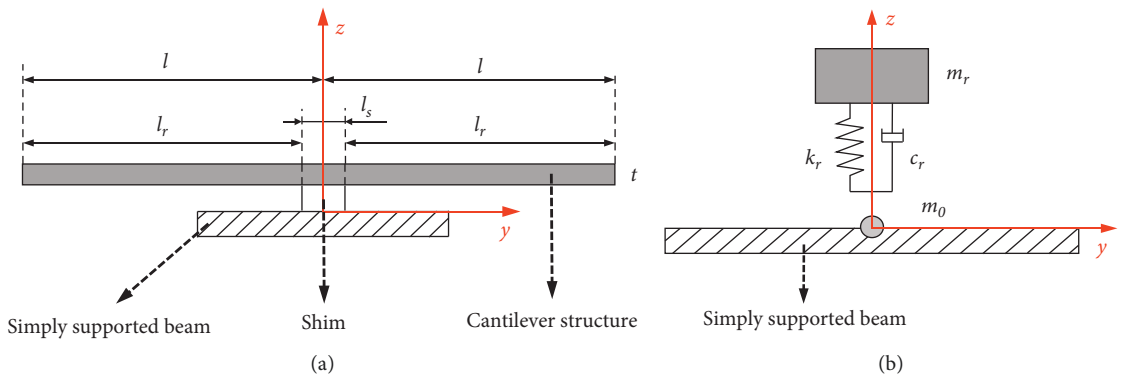

FIGURE 2: (a) Schematic diagram of the beam-like resonator. (b) Simplified equivalent system.

frequencies, the beam-like resonators can be treated as a "mass-spring-mass" system with a damping component [23]. The parameters of the equivalent system can be denoted as m_0, m_r, k_r, and c_r, as shown in Figure 2(b), where m_0 is the additional lumped mass attached to the host beam at the point where the beam-like resonator is mounted and m_r, k_r, and c_r are the effective mass, effective stiffness, and effective damping of the beam-like resonator, respectively. To simplify the calculation, the damping c_r is set to be 0.1 N s/m.

Supposing that Young's modulus of the beam-like resonator is E_r and the density is ρ_r, within the low-frequency range, the relevant parameters of its equivalent system [24] can be expressed as follows:

$$m_0 = \rho_r A_r l_s + 0.395\rho_r A_r (2l_r), \tag{1}$$

$$m_r = 0.605\rho_r A_r (2l_r), \tag{2}$$

$$k_r = 14.953 \frac{E_r I_r}{l_r^3}, \tag{3}$$

where $A_r = b_r t_r$ is the cross-sectional area of the beam-like resonator, and $I_r = b_r t_r^3/12$ is the second axial moment of area of the beam-like resonator. The resonance frequency of the beam-like resonator can then be calculated by the following expression:

$$\begin{aligned} f_r &= \frac{1}{2\pi}\sqrt{\frac{k}{m}} \\ &= \left(\frac{1}{2\pi}\right)\left(\frac{3.515}{l_r^2}\right)\sqrt{\frac{E_r I_r}{\rho_r A_r}} \\ &= \left(\frac{1}{4\pi}\right)\left(\frac{3.515 t_r}{l_r^2}\right)\sqrt{\frac{E_r}{3\rho_r}}. \end{aligned} \tag{4}$$

Next, the locally resonant beam can be simplified into an equivalent theoretical model, as shown in Figure 3. m_{0ij}, m_{ij}, k_{ij}, and c_{ij} represent the attached mass, effective mass, effective stiffness, and effective damping of the beam-like resonator in the jth resonator of the ith unit, respectively.

2.2. Formulations. Ignoring the influence of shear deformation and the moment of inertia of the section around the neutral axis, the beam is considered as a Bernoulli–Euler beam. The finite locally resonant beam is a continuous-discrete coupled system. According to the vibration principle, the coupling vibration equation of the continuous beam with discrete resonators can be written as follows:

$$\begin{aligned} \rho A \frac{\partial^2 w(x,t)}{\partial t^2} + EI \frac{\partial^4 w(x,t)}{\partial x^4} &= F(t)\delta(x - x_0) \\ &+ \left[\sum_{i=1}^{M}\sum_{j=1}^{N} F_{ij}(x_{ij},t) + \omega^2 m_{0ij} w(x_{ij},t)\right]\delta(x - x_{ij}), \end{aligned} \tag{5}$$

$$\begin{aligned} &m_{ij}\ddot{u}_{ij}(x_{ij},t) + c_{ij}\dot{u}_{ij}(x_{ij},t) + k_{ij}u_{ij}(x_{ij},t) \\ &= m_{0ij}\ddot{w}_{ij}(x_{ij},t) + c_{ij}\dot{w}_{ij}(x_{ij},t) + k_{ij}w(x_{ij},t), \end{aligned} \tag{6}$$

with

$$\begin{cases} F_{ij} = F_{kij} + F_{cij}, \\ F_{kij} = -k_{ij}\left[w(x_{ij},t) - u_{ij}(x_{ij},t)\right], \\ F_{cij} = -c_{ij}\left[\dot{w}(x_{ij},t) - \dot{u}_{ij}(x_{ij},t)\right], \\ u_{ij}(x_{ij},t) = U_{sij}\sin\omega t + U_{cij}\cos\omega t, \end{cases} \tag{7}$$

where ρ, E, and I are the density, Young's modulus, and second axial moment of area of the simply supported beam, respectively. $w(x,t)$ is the transverse vibration displacement of the locally resonant beam at coordinate x. $F(t)$ is the point force applied at the position of x_0, which can be expressed as $F(t) = F_0 \sin \omega t$. $F_{ij}(x_{ij},t)$ is the reaction force of the resonator at the coordinate of x_{ij} on the beam; the reaction force of the resonator contains the spring's reaction force F_{kij} and the damping reaction force F_{cij}. δ is the Dirac function. $u_{ij}(x_{ij},t)$ is the displacement of the resonator mass at coordinate x_{ij}, where U_{sij} and U_{cij} represent the sine and cosine components of $u_{ij}(x_{ij},t)$ at the coordinate of x_{ij}.

By employing the modal superposition method, the transverse vibration displacement of the simply supported beam can be expressed as follows:

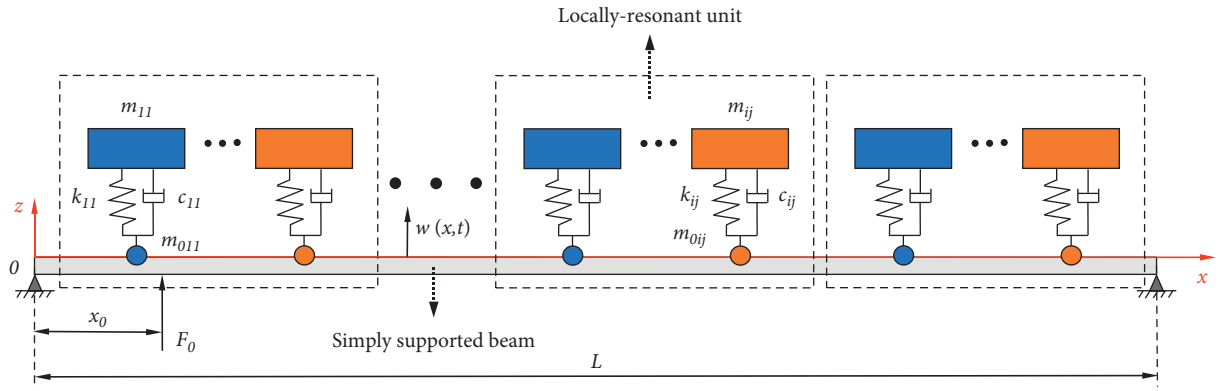

FIGURE 3: A simplified model of the finite locally resonant beam.

$$w(x,t) = \sum_{m=1}^{\infty} W_m(x)\left(W_{sm}\sin\,\omega t + W_{cm}\cos\,\omega t\right), \tag{8}$$

where m refers to the modal order, $W(x) = \sin(m\pi x/L)$ is the mode shape function, W_{sm} and W_{cm} are the sine and cosine components of the modal displacement, and ω is the excitation angular frequency.

After multiplying both sides of (5) by $\sin(n\pi x/L)$ and integrating x from 0 to L, (5) can be written as follows:

$$\begin{aligned}&\left[-\rho A\omega^2 + EI\left(\frac{m\pi}{L}\right)^4\right]\left(\frac{L}{2}\right)\left(W_{sm}\sin\,\omega t + W_{cm}\cos\,\omega t\right) = F(t)\sin\left(\frac{n\pi x_0}{L}\right)\\ &-\sum_{i=1}^{M}\sum_{j=1}^{N}\left[\left(k_{ij} - \omega^2 m_{0ij}\right)w\left(x_{ij},t\right) - k_{ij}u_{ij}\left(x_{ij},t\right)\right]\sin\left(\frac{n\pi x_{ij}}{L}\right) - \sum_{i=1}^{M}\sum_{j=1}^{N}c_{ij}\left[\dot{w}\left(x_{ij},t\right) - \dot{u}_{ij}\left(x_{ij},t\right)\right]\sin\left(\frac{n\pi x_{ij}}{L}\right).\end{aligned} \tag{9}$$

Taking the Q-order mode of the beam to participate in the calculation, (9) can be converted into the matrix form as follows:

$$\mathbf{Gq} = \mathbf{F}, \tag{10}$$

where $\mathbf{G}$ is the coefficient matrix, F is the force vector, and $\mathbf{q}$ is the unknown vector of the coupled equations needing to be solved, given by the following equation:

$$\mathbf{q} = \begin{bmatrix}\mathbf{W}_s\\ \mathbf{W}_c\\ \mathbf{U}_s\\ \mathbf{U}_c\end{bmatrix}, \tag{11}$$

where $\mathbf{W}_s = [W_{s1},\cdots,W_{sQ}]^{\mathrm{T}}$ and $\mathbf{W}_c = [W_{c1},\ldots,W_{cQ}]^{\mathrm{T}}$, $\mathbf{U}_s = [U_{s1},\ldots,U_{sMN}]^{\mathrm{T}}$ and $\mathbf{U}_c = [U_{c1},\ldots,U_{cMN}]^{\mathrm{T}}$.

Matrix $\mathbf{G}$ can be written as follows:

$$\mathbf{G} = \begin{bmatrix}\mathbf{K}_1 & \mathbf{C}_1 & \mathbf{K}_2 & \mathbf{C}_2\\ -\mathbf{C}_1 & \mathbf{K}_1 & -\mathbf{C}_2 & \mathbf{K}_2\\ \mathbf{K}_3 & \mathbf{C}_3 & \mathbf{K}_4 & \mathbf{C}_4\\ -\mathbf{C}_3 & \mathbf{K}_3 & -\mathbf{C}_4 & \mathbf{K}_4\end{bmatrix}, \tag{12}$$

with

$$\begin{cases}\mathbf{w}_{ij} = \left[\sin\dfrac{\pi x_{ij}}{L},\ \sin\dfrac{2\pi x_{ij}}{L},\ldots,\ \sin\dfrac{Q\pi x_{ij}}{L}\right]^T,\\ \mathbf{K}_1 = \left(\dfrac{l}{2}\right)\mathrm{diag}\left(\Lambda_1,\Lambda_2,\ldots,\Lambda_Q\right) + \sum_{i=1}^{Q}\sum_{j=1}^{Q}\left(k_{ij} - m_{0ij}\omega^2\right)\mathbf{w}_{ij}\mathbf{w}_{ij}^T,\\ \mathbf{C}_1 = -\sum_{i=1}^{Q}\sum_{j=1}^{Q}c_{ij}\omega\mathbf{w}_{ij}\mathbf{w}_{ij}^T,\end{cases} \tag{13}$$

where $\Lambda_i = -\rho A\omega^2 + EI\,(i\pi/L)^4$. i represents the modal order, which is in the range of 0–Q.

Stiffness matrices $\mathbf{K}_2$, $\mathbf{K}_3$, and $\mathbf{K}_4$ can be written as follows:

$$\mathbf{K}_2 = -\begin{bmatrix} k_{11}\sin\dfrac{\pi x_{11}}{L} & \cdots & k_{\mathrm{MN}}\sin\dfrac{\pi x_{\mathrm{MN}}}{L} \\ \vdots & \ddots & \vdots \\ k_{11}\sin\dfrac{Q\pi x_{11}}{L} & \cdots & k_{\mathrm{MN}}\sin\dfrac{Q\pi x_{\mathrm{MN}}}{L} \end{bmatrix},$$

$$\mathbf{K}_3 = \begin{bmatrix} \left(k_{11} - m_{011}\omega^2\right)\sin\dfrac{\pi x}{L} & \cdots & \left(k_{11} - m_{011}\omega^2\right)\sin\dfrac{Q\pi x}{L} \\ \vdots & \ddots & \vdots \\ \left(k_{\mathrm{MN}} - m_{0\mathrm{MN}}\omega^2\right)\sin\dfrac{\pi x}{L} & \cdots & \left(k_{\mathrm{MN}} - m_{0\mathrm{MN}}\omega^2\right)\sin\dfrac{Q\pi x}{L} \end{bmatrix}, \tag{14}$$

$$\mathbf{K}_4 = -\begin{bmatrix} k_{11} - m_{11}\omega^2 & \cdots & 0 \\ \vdots & \ddots & \vdots \\ 0 & \cdots & k_{\mathrm{MN}} - m_{\mathrm{MN}}\omega^2 \end{bmatrix}.$$

Matrix $\mathbf{K}_1$ contains the stiffness contribution of resonators to the beam. Matrices $\mathbf{K}_2$ and $\mathbf{K}_3$ represent the coupled effects of resonators on the finite locally resonant beam.

Damping matrices $\mathbf{C}_2$, $\mathbf{C}_3$, and $\mathbf{C}_4$ can be written as follows:

$$\mathbf{C}_2 = \begin{bmatrix} c_{11}\omega\,\sin\dfrac{\pi x_{11}}{L} & \cdots & c_{\mathrm{MN}}\omega\,\sin\dfrac{\pi x_{\mathrm{MN}}}{L} \\ \vdots & \ddots & \vdots \\ c_{11}\omega\,\sin\dfrac{Q\pi x_{11}}{L} & \cdots & c_{\mathrm{MN}}\omega\,\sin\dfrac{Q\pi x_{\mathrm{MN}}}{L} \end{bmatrix},$$

$$\mathbf{C}_3 = -\begin{bmatrix} c_{11}\omega\,\sin\dfrac{\pi x_{11}}{L} & \cdots & c_{11}\omega\,\sin\dfrac{Q\pi x_{\mathrm{MN}}}{L} \\ \vdots & \ddots & \vdots \\ c_{\mathrm{MN}}\omega\,\sin\dfrac{\pi x_{11}}{L} & \cdots & c_{\mathrm{MN}}\omega\,\sin\dfrac{Q\pi x_{\mathrm{MN}}}{L} \end{bmatrix}, \tag{15}$$

$$\mathbf{C}_4 = \begin{bmatrix} c_{11}\omega & \cdots & 0 \\ \vdots & \ddots & \vdots \\ 0 & \cdots & c_{\mathrm{MN}}\omega \end{bmatrix}.$$

Matrices $\mathbf{C}_1$, $\mathbf{C}_2$, and $\mathbf{C}_3$ represent the effects of the damping of resonators on the locally resonant beam.

The right side of the matrix (10) represents the force vector acting on the beam surface at the coordinate of x_0, which can be expressed as follows:

$$\mathbf{F} = \left[\mathbf{F}_1, 0_{1\times(Q+\mathrm{MN})}\right]^{\mathrm{T}}, \tag{16}$$

where

$$\mathbf{F}_1 = F_0\left[\sin\frac{\pi x_0}{L},\ \sin\frac{2\pi x_0}{L}, \ldots,\ \sin\frac{Q\pi x_0}{L}\right]^{\mathrm{T}}. \tag{17}$$

Considering the frequency of harmonic force $f = \omega/2\pi$, the solution of the unknown vector $\mathbf{q}$ at excitation frequency f can be obtained by the following equation:

$$\mathbf{q} = \mathbf{G}^{-1}\mathbf{F}. \tag{18}$$

Furthermore, the unknown matrix at every excitation frequency $[f_1, f_2, \ldots, f_e]$ can be described as follows:

$$\mathbf{q} = \begin{bmatrix} \mathbf{W}_s^1 & \mathbf{W}_s^2 & \cdots & \mathbf{W}_s^e \\ \mathbf{W}_c^1 & \mathbf{W}_c^2 & \cdots & \mathbf{W}_c^e \\ \mathbf{U}_s^1 & \mathbf{U}_s^2 & \cdots & \mathbf{U}_s^e \\ \mathbf{U}_c^1 & \mathbf{U}_c^2 & \cdots & \mathbf{U}_c^e \end{bmatrix}, \tag{19}$$

where $\mathbf{q}$ is a $2\,(Q + \mathrm{MN}) \times e$ dimensional unknown matrix.

Based on equations (8), (12), and (21), defining the modal shape vector $\mathbf{W}_m$, the matrices $\mathbf{q}_{ws}$ and $\mathbf{q}_{wc}$ can be expressed as follows:

$$\mathbf{W}_m = \left[\sin\left(\frac{\pi x}{L}\right),\ \sin\left(\frac{2\pi x}{L}\right), \ldots,\ \sin\left(\frac{Q\pi x}{L}\right)\right], \tag{20}$$

$$\mathbf{q}_{ws} = \begin{bmatrix} \mathbf{W}_s^1 & \mathbf{W}_s^2 & \cdots & \mathbf{W}_s^e \end{bmatrix} = \begin{bmatrix} W_{s1}^1 & W_{s1}^2 & \cdots & W_{s1}^e \\ W_{s2}^1 & W_{s2}^2 & \cdots & W_{s2}^e \\ \vdots & \vdots & \ddots & \vdots \\ W_{sQ}^1 & W_{sQ}^2 & \cdots & W_{sQ}^e \end{bmatrix}, \tag{21}$$

$$\mathbf{q}_{wc} = \begin{bmatrix} \mathbf{W}_c^1 & \mathbf{W}_c^2 & \cdots & \mathbf{W}_c^e \end{bmatrix} = \begin{bmatrix} W_{c1}^1 & W_{c1}^2 & \cdots & W_{c1}^e \\ W_{c2}^1 & W_{c2}^2 & \cdots & W_{c2}^e \\ \vdots & \vdots & \ddots & \vdots \\ W_{cQ}^1 & W_{cQ}^2 & \cdots & W_{cQ}^e \end{bmatrix}. \tag{22}$$

Considering the principle of the modal superposition method again and combining (8), (20), (21), and (22), the transverse amplitude vector w at coordinate x on the finite beam can be written as follows:

$$\mathbf{w} = \begin{bmatrix} w_1 & w_2 & \cdots & w_e \end{bmatrix}, \tag{23}$$

where

$$w_i = \sqrt{\left[\sum_{j=1}^{Q} W_{sj}^i \sin\left(\frac{j\pi x}{L}\right)\right]^2 + \left[\sum_{j=1}^{Q} W_{cj}^i \sin\left(\frac{j\pi x}{L}\right)\right]^2}. \tag{24}$$

The two parts under the radical sign in (24) represent the sine and cosine components of the amplitude, respectively. Then, the velocity amplitude vector of the finite beam at x at each excitation frequency can be calculated by the following equation:

$$\mathbf{v} = \omega\mathbf{w}, \tag{25}$$

Table 1: Parameters of the finite beam.

L (mm)	B (mm)	H (mm)	E (Pa)	ρ (kg·m^{-3})	ν
1160	50	5	6.8×1010	2860	0.33

where each element $v(f)$ in the vector $\mathbf{v}$ corresponds to the velocity amplitude at a particular excitation frequency.

Here, the average velocity level which could represent the vibration energy is used to assess the vibration control effect. The surface average velocity levels can be given by the following equation:

$$Lv(f) = 10\lg\frac{V(f)}{V_0}, \tag{26}$$

where V_0 is the reference vibration speed in calculating, and $V_0 = 5\times10^{-8}$m/s.

3. Results and Discussion

To investigate the control performance with regard to low-frequency vibration, some numerical examples of finite locally resonant beams are presented and discussed. It is known that the periodic arrangement and antiresonance effect of locally resonant units is the main factor in elastic wave attenuation. Therefore, we first consider finite locally resonant beams with different resonator length, thickness, and width. Next, we will cover the periodic number of the locally resonant units required to suppress the propagation of elastic waves, as well as the minimum periodic number of units to form a bandgap. Specifically, the root mean square of the average surface velocity level is used to define the average velocity response of the whole finite beam. Assuming that the measuring points are set on the beam and combined with (26), the average velocity response of the whole finite beam is defined as follows:

$$L\overline{v}(f) = \sqrt{\frac{\sum_{i=1}^{S}\left[Lv_i(f)\right]^2}{S}}, \tag{27}$$

where S is the number of selected points. $Lv_i(f)$ is the average vibration speed level of the ith measuring point at frequency f.

3.1. Influences of the Locally Resonant Unit. To provide a preliminary insight into the influences of the locally resonant unit on the vibration attenuation properties, the finite locally resonant beam with a simply supported boundary is established, and the parameters of the beam are shown in Table 1 where L, B, H, E, ρ, and ν represent length, width, thickness, Young's modulus, density, and Poisson's ratio of the finite beam, respectively. Considering the space occupied by the resonators, reducing the additional mass as much as possible and ensuring the vibration attenuation properties. Assuming that twelve locally resonant units are distributed uniformly on the simply supported beam, consider that the unit contains one or two beam-like resonators to form a single-resonator unit and double-resonator unit. To realize single-frequency and multifrequency vibration control below 500 Hz, two different beam-like resonators are designed, and the structural parameters and resonance frequency (calculated by (4)) of two types of beam-like resonators are shown in Table 2 where $2l$, h, and w represent the total length, thickness, and width of the beam-like resonators, respectively. The beam-like resonators are made of steel with material density $\rho_r = 7930$ kg/m3, Young's modulus $E_r = 1.34\times10^{11}$ Pa, and Poisson's ratio $v_r = 0.3$. After calculation, the mass of the beam is about 829.4 g, and the mass of resonator1 and resonator2 account for 4.59% and 4.97% of the beam mass, respectively.

Table 2: Parameters and resonance frequency of beam-like resonators.

	$2l$ (mm)	h (mm)	w (mm)	m (g)	f_r (Hz)
Resonator1	120	2	20	38.1	401.57
Resonator2	130	2	20	41.2	339.89

Considering a unit excitation force applied at $3L/20$ on the simply supported beam with the frequency range of 0–600 Hz, the influences of locally resonant units on the vibration characteristics of the finite beam are analyzed. By using (27), the average velocity responses $L\overline{v}(f)$ of the locally resonant beams with two types of units can be obtained (see Figure 4). Figure 4 shows some similar trends: the resonance frequencies of beams can be decreased by adding the resonator, while the effects on lower resonance frequencies are weaker than on higher ones. In addition, one minimum point in the average velocity response (see Figure 4(a)) is much lower than other frequency points, and the corresponding frequencies of minimum point are 401.6 Hz, two minimum points in Figure 4(b) correspond to 401.6 Hz and 340 Hz. Noted that the frequencies of minimum points correspond to the resonance frequencies of Resonator1 and Resonator2 (as shown in Table 1); the phenomenon may be called locally resonant bandgap [3]. This may be the main effect of boundary conditions on the bandgap of finite compared to infinite locally resonant beams.

To further verify the correctness of theoretical results concerning the low-frequency vibration characteristics of the finite beam, taking the beam in Figure 4(a) as an example, the theory to simulate the average velocity response in this paper is examined by using the finite element software package ANSYS Workbench R19.0. The comparisons of theoretical result and finite element result for the finite beam without resonator are shown in Figure 5, and good agreements can be found in the figure. The positions and sizes of the resonance peaks in Figure 5 are basically the same, and the errors at other frequency positions may be due to the average velocity response calculated by several measuring points cannot completely replace the results of the whole surface for the finite beam.

For further insight into the vibration characteristics of a locally resonant beam within a bandgap, taking the host beam and the locally resonant beam in Figure 4(a) as examples, the vibration responses of the host beam and the locally resonant beam are numerically simulated using the finite element software of ANSYS. The model of a finite

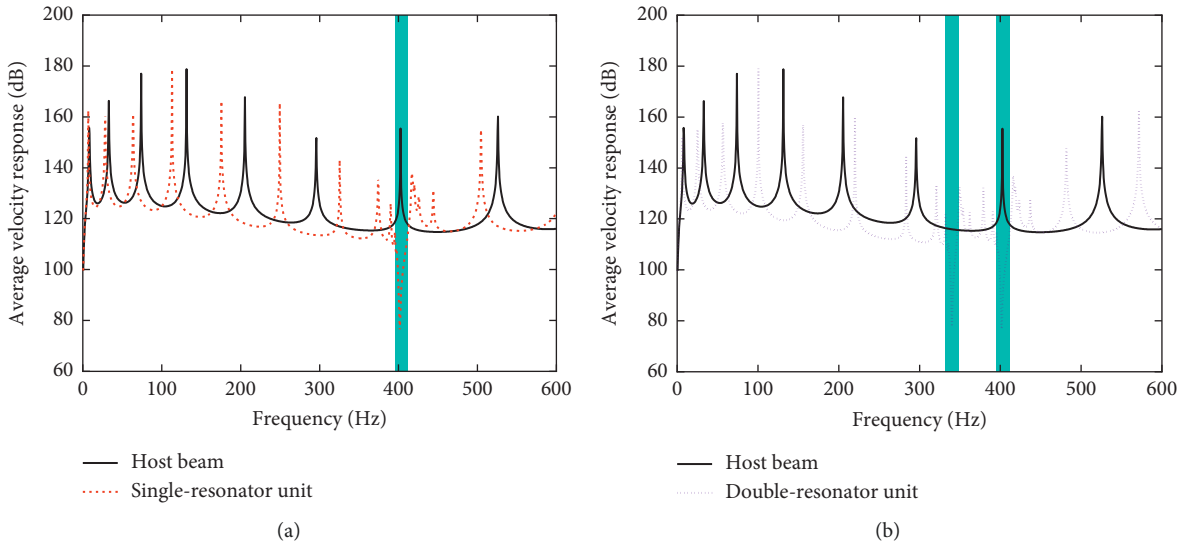

Figure 4: Average velocity response curves of the finite locally resonant beam with (a) single-resonator units contain Resonator1 (401.57 Hz) and (b) double-resonator units contain Resonator1 (401.57 Hz) and Resonator2 (339.89 Hz).

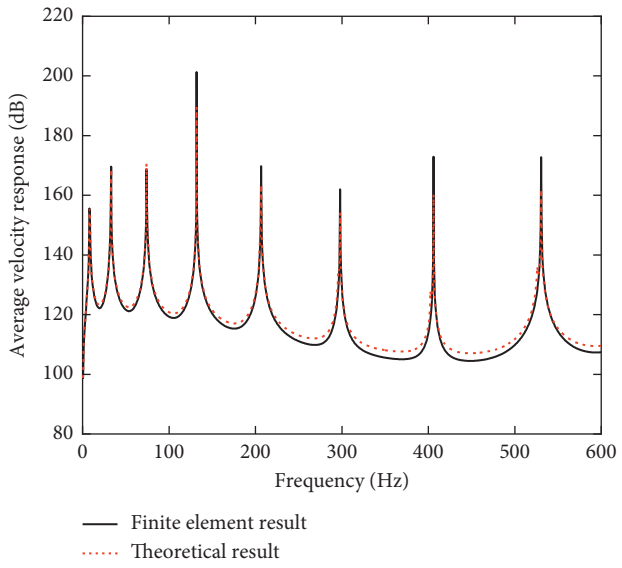

Figure 5: The comparison of average velocity response by theory and finite element method for the finite beam.

beam with periodic arrays of Resonator1 under simply supported boundary conditions is illustrated in Figure 6. Figure 7 shows the displacement profiles of the beam without resonators and the locally resonant beam at 401.6 Hz. The figure proves the suppression of the bandgap on the vibration of the simply supported beam, the maximum amplitude of the finite beam without a resonator is 0.43 mm (see Figure 7(a)), and the maximum amplitude of the finite locally resonant beam is about 2.92×10^{-3} mm (see Figure 7(b)). The vibration responses over almost the whole surface of the locally resonant beam are much lower than that of the beam without resonators. This may be due to the periodic arrangement of the resonators and antiresonance effects of locally resonant units, which is different from the traditional bandgap mechanism [25, 26]. Hence, the finite element results can verify the vibration attenuation performance of bandgaps.

3.2. Influences of the Number and Parameters of Resonators. It is of interest to investigate the effects of the number and parameters of resonators on vibration and noise control. In order to identify the bandgap width, one assumes the center frequency, the upper and lower bound frequency, and the vibration attenuation to be f_{R0}, f_{RU} and f_{RL}, and ΔLv, respectively. For example, supposing the center frequency is $f_{R0} = 401.6$Hz, $Lv\,(f_{R0}) = 75.46$dB, and selecting $\Delta Lv = 40$ dB, f_{RU} and f_{RL} can be calculated by the evaluation index: $Lv\,(f_{RU}) \geq Lv(f_{R0}) + \Delta Lv$, $Lv\,(f_{RU}) \geq Lv\,(f_{R0}) + \Delta Lv$.

First, we will discuss the influence of the length of resonators on the bandgap characteristics of the finite locally resonant beam. Taking the finite locally resonant beam with twelve Resonator1 as an example, then reducing and increasing the length of Resonator1 by 10 mm, and calculating the average velocity response of the finite locally resonant beam with resonators of different lengths. The bandgaps of finite locally beams are labeled by the shaded area in Figures 8(a)–8(c). From the comparison between Figures 8(a)–8(c), several significant results can be obtained: the resonance frequencies of the finite locally resonant beam are decreased by increasing the length of the beam-like resonator. When the length of the beam-like resonator changes from 110 mm to 120 mm and 130 mm, the average velocity response $L\overline{v}(f)$ at the center frequency of the bandgap increases from 75.46 dB to 76.95 dB to 78.35 dB, and the vibration attenuation tends to decrease. The width of the bandgaps correspond to the three kinds of resonator are 16.3 Hz, 16.4 Hz, and 16.5 Hz, so the resonator length has little influence on bandgap width. From 110 mm to 130 mm, the mass increases by 3 g for every 10 mm in length, which is

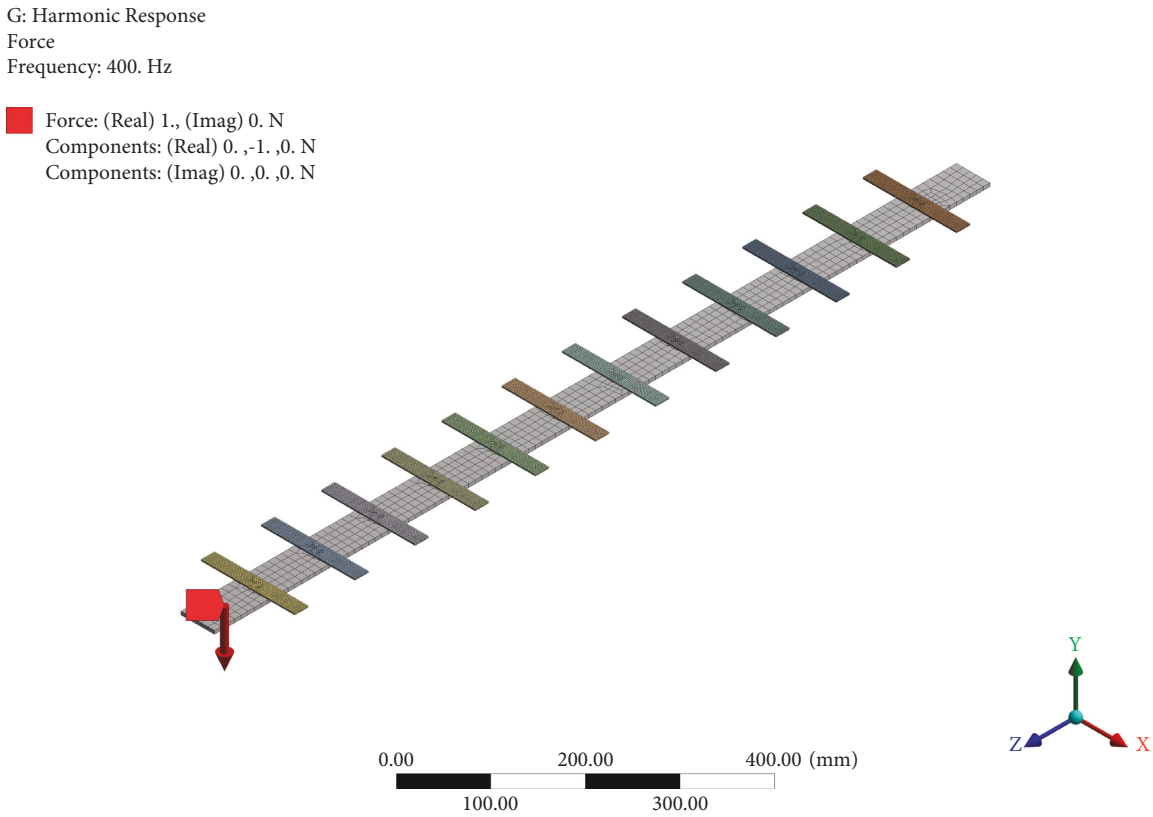

Figure 6: Structural model diagram of the finite beam with periodic arrays of Resonator1.

about 0.375% of the beam mass; therefore, it is impossible to change the bandgap width due to the small change in mass.

Next, we will discuss the influence of the thickness of resonators on the bandgap characteristics of the finite locally resonant beam. Taking the thickness of Resonator1 as the initial thickness, and increasing and decreasing its thickness by 0.2 mm, then calculating the average velocity response of the finite locally resonant beam with three types of resonators as shown in Figure 9. It can be seen that resonator thickness has a significant influence on the average velocity response of the beam in terms of the following aspects: (i) the increase in resonator thickness causes the resonance frequency of the finite locally resonant beam to shift to higher frequencies, with weaker effects on the lower resonance frequencies than on the higher ones. (ii) The average velocity responses $L\overline{v}(f)$ at the center frequencies of the bandgap are 79.65 dB (1.8 mm thick), 75.46 dB (2 mm thick), and 71.66 dB (2.2 mm thick), so for every 0.2 mm increase in resonator thickness, the average velocity response at the minimum point is reduced by about 4 dB.

In the range of 0–600 Hz, the bandgaps induced by the resonance effect are labeled in Figures 9(a)–9(c), with bandgap frequency ranges of 354.9–370.4 Hz, 395.4–412.7 Hz, and 432.4–455.2 Hz; the bandgaps correspond to the resonance frequency of the resonator with a thickness of 1.8 mm (361.42 Hz), resonator with a thickness of 2.0 mm (401.57 Hz), and resonator with a thickness of 2.2 mm (441.73 Hz). Meanwhile, (2) and (4) show a positive correlation between resonator thickness and resonance frequency. With increased resonator thickness, resonator mass also increases to enhance the resonance effect of coupling with the beam; this is the main reason for the improvement of the vibration attenuation performance of the bandgap. A comparison between Figures 8 and9 shows that the resonator thickness is more sensitive to bandgap than resonator length. Hence, the thickness should be adjusted more precisely when controlling the resonance frequency of resonators.

We also analyzed the influence of resonator width on the bandgap characteristics of the finite locally resonant beam. According to (2), the resonance frequency of a resonator is independent of its width. However, resonator width is positive to the mass, so that bandgap characteristics can be controlled by the width. Assuming that the width of Resonator1 is the initially calculated width, and increases and decreases its thickness by 10 mm, we will discuss three examples of the finite beam with periodic arrays of resonators. Several obvious phenomena can be observed in Figure 10: (i) the resonance frequencies of the finite locally resonant beam decrease with increasing resonator width and compared with the higher resonance frequency, the lower resonance frequency changes less. (ii) The center frequencies of the bandgaps are not changed, while the bandgap width increases from 11.8 Hz to 17.3 Hz to 24.5 Hz, and the vibration response at the center frequency of the bandgaps is 80.09 dB, 75.46 dB, and 67.37 dB. Every 10-mm increase in the width of a resonator increases its mass by 19 g, as shown in Table 1. This remarkable change in mass enhances the

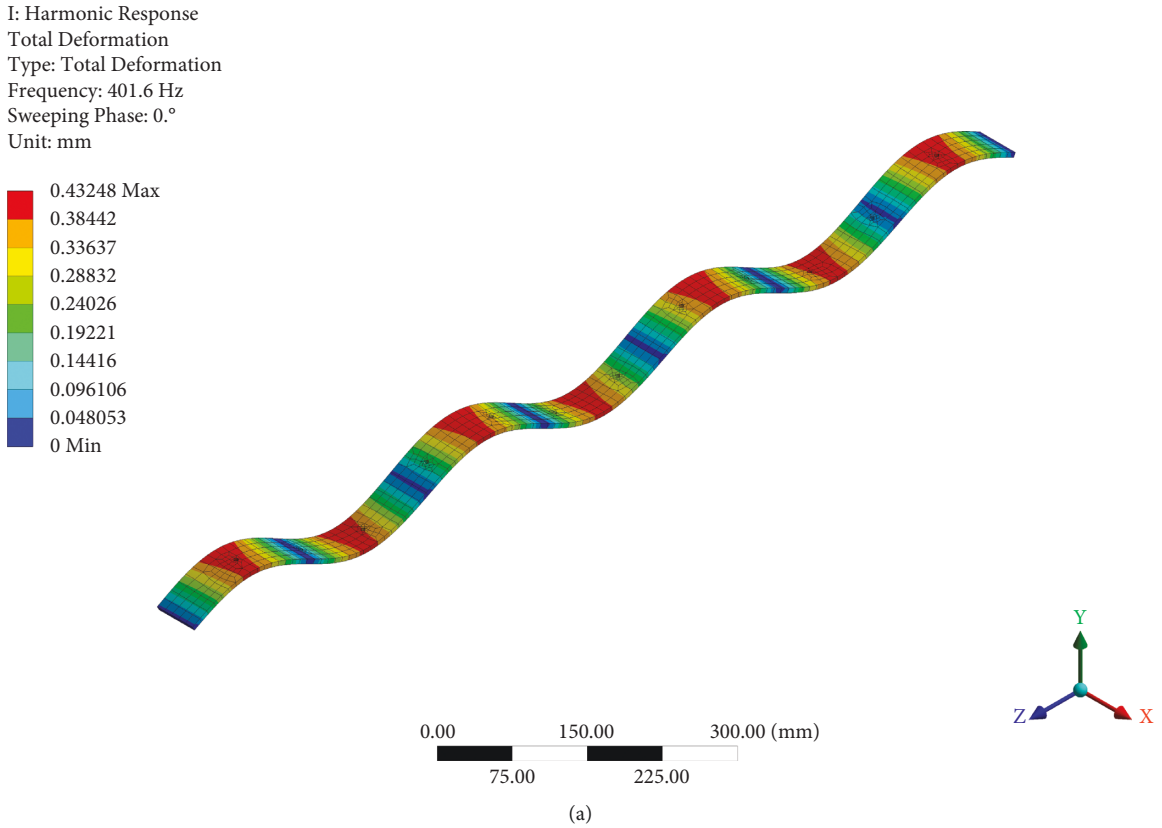

(a)

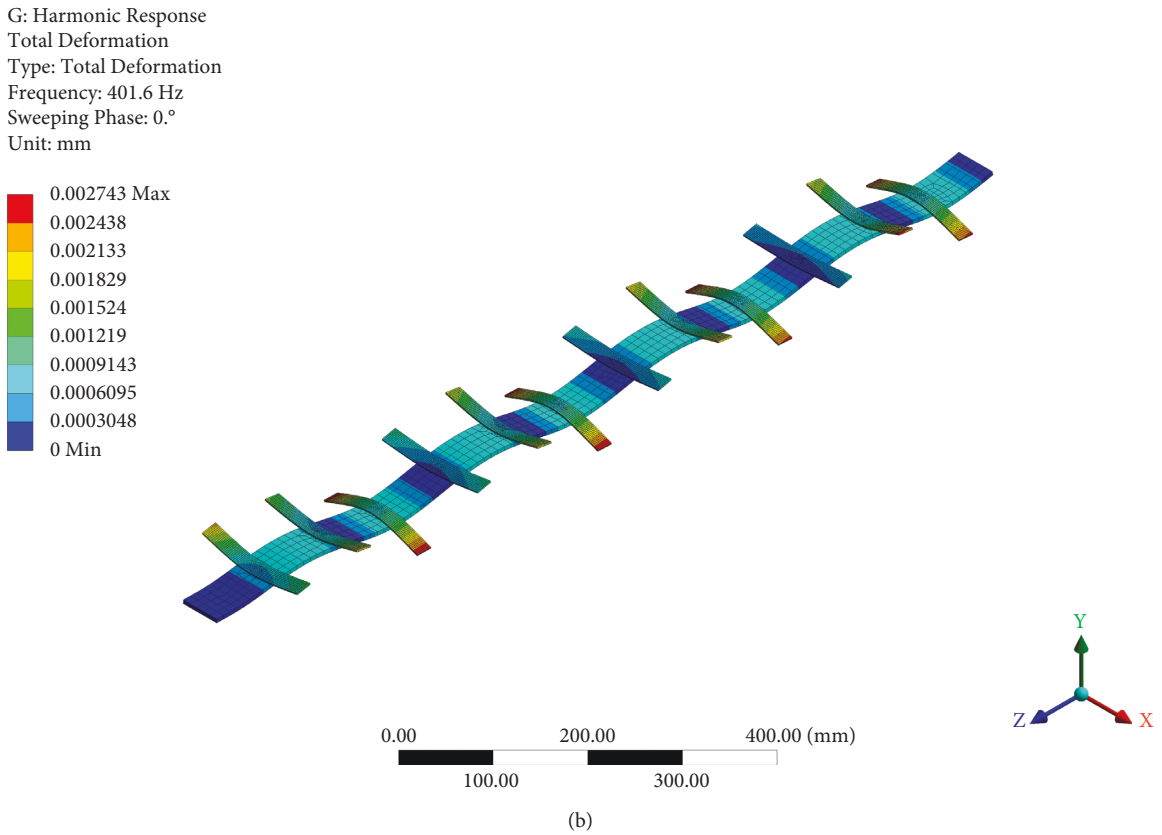

(b)

Figure 7: The displacement profiles of (a) the finite beam and (b) the finite beam with periodic arrays of Resonator1 (401.57 Hz) at 401.6 Hz.

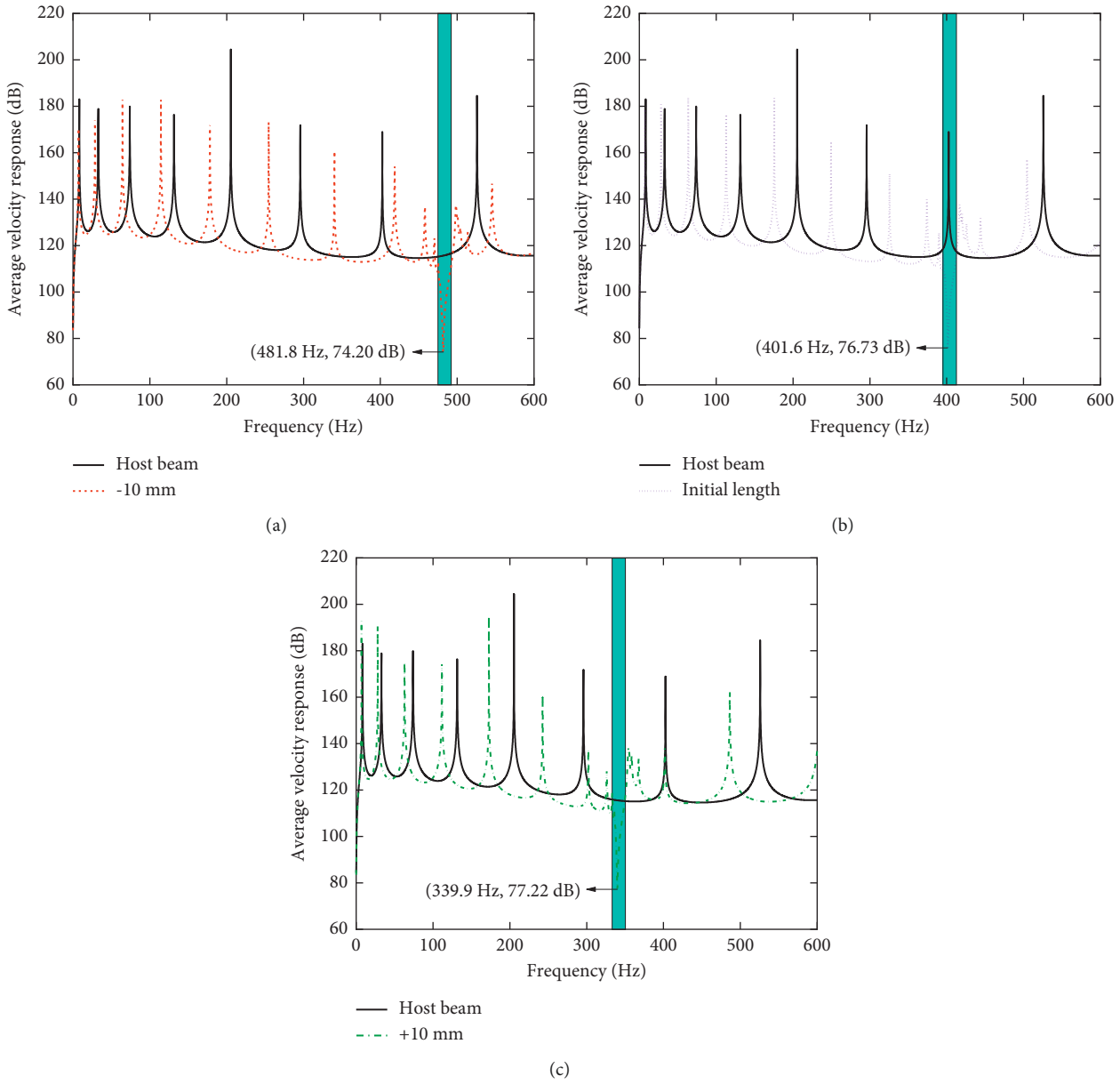

Figure 8: Influence of the beam-like resonator's length on the vibration properties of the locally resonant beam.

resonance effect in the finite locally resonant beam. Furthermore, as resonator width increases, the bandgap is widened and the vibration attenuation performance of the bandgap is improved, which can also be attributed to the change in mass caused by the change in resonator width.

To further investigate the effects of periodic units' number on the bandgap, we established a dynamic model of the finite beam with several Resonator1 (see Figure 11), with a unit harmonic force applied at $L/20$ and the measuring point at $19L/20$. The average velocity response at the measuring point is employed to analyze the elastic wave attenuation characteristics between the force application point and the measuring point.

The unit harmonic force F_0 represents the input signal, and the velocity response of the measuring point represents the output signal by $Lv_P(f)$. Given a frequency range of 0–600 Hz and calculating the vibration response diagram of the measuring point on the beam based on 0–26 periodic units, one assumes the number of periods is represented by N_R. Comparing the numerical results of $Lv_P(f)$ under different periodic units by formulations in Section 2.2, the conclusion that there is a bandgap that meets the demand for vibration reduction as periods' numbers are above 9 can be drowned. Therefore, by analyzing the average velocity response at the measuring point when N_R is 1 and 9, it can be confirmed that the periodic structure is necessary for the formation of bandgaps, and the average vibration attenuation at the bandgap when $N_R \geq 9$ are calculated in Figure 12(b).

From Section 3.1, periodic resonators can affect the vibration performance of the finite beam. In Figure 12(a), it is clear that a

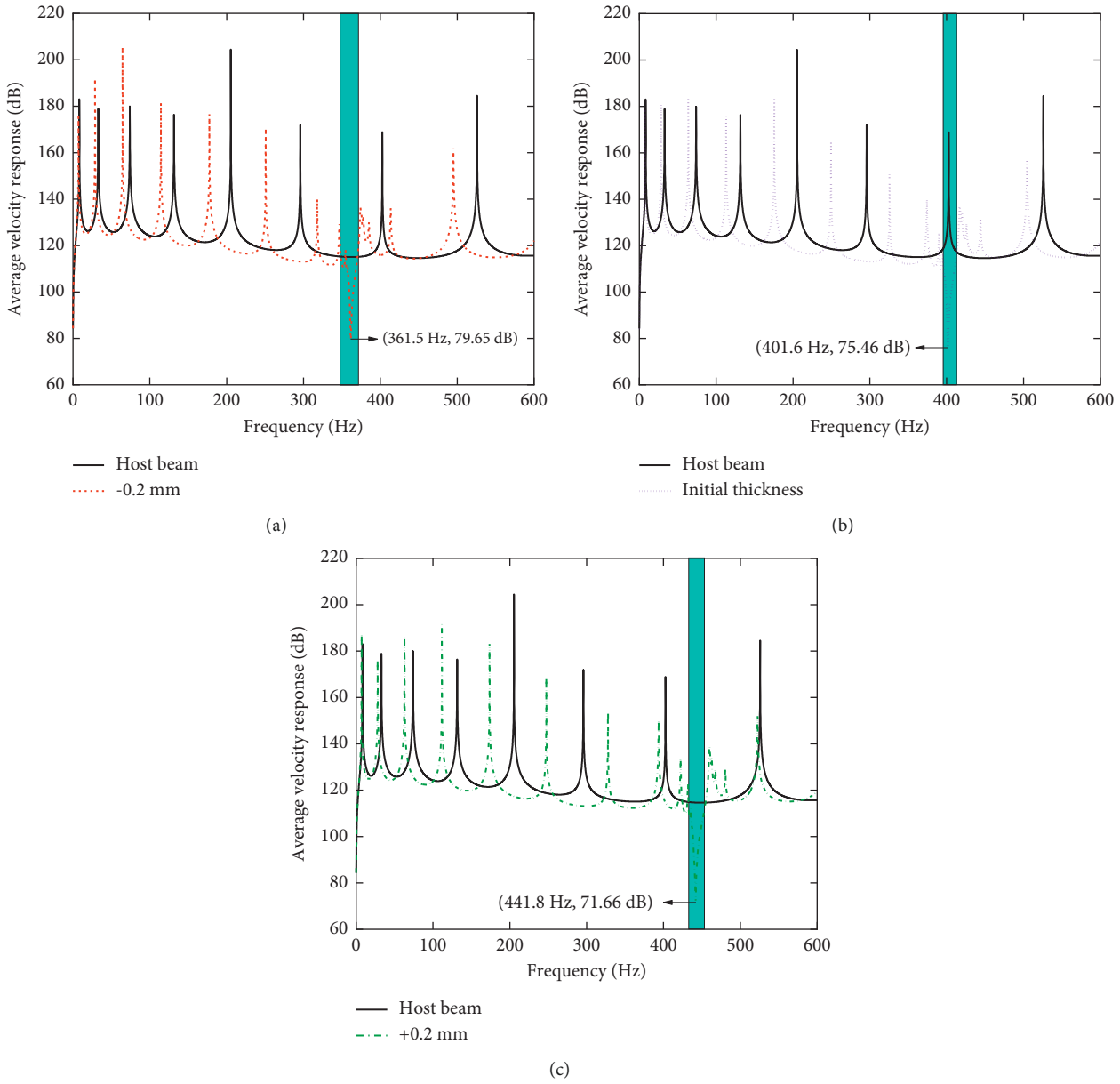

Figure 9: Influence of the beam-like resonator's thickness on the vibration properties of the locally resonant beam.

single-resonator also has a certain inhibitory effect on the vibration of the finite beam, and all resonance peaks of the finite beam are reduced, the resonance frequency is decreased and the effects on lower resonance frequency is smaller than higher resonance frequency, which is similar to the periodic resonators. However, the finite beam with a single resonator does not have a bandgap that corresponds to the resonance frequency of the resonator like the finite locally resonant beam with periodic resonators. In Figure 12(b), as the number of unit increases, the average vibration attenuation within the bandgap gradually shows an upward trend and then to be stable. When N_R varied from 9 to 12, the average vibration attenuation changes faster than N_R in the range of 13 to 26 and gradually tends to converge.

Additional resonators appeared to decrease the resonance frequency of the finite beam, and the resonance frequency of the finite locally resonant beam with multiple resonators was lower than that of the finite beam with a single resonator, which may be due to the increasing mass of the total resonators affecting the mass matrix of the coupling equation. Because the periodic structure has richer wave-filtering properties, waves cannot propagate freely within the frequency range of the bandgap. In Figure 12(a), a bandgap only exists in the finite locally resonant beam with periodic arrays of resonators instead of the finite beam with a single resonator, and the results confirmed that the periodic structure is the reason for bandgap formation. Trends that vibration attenuation is proportional to the number of units shown in Figure 12(b) illustrates the effect of the periodic number of units on the transfer function when the parameters of a periodic unit are fixed. When N_R increases, the range of

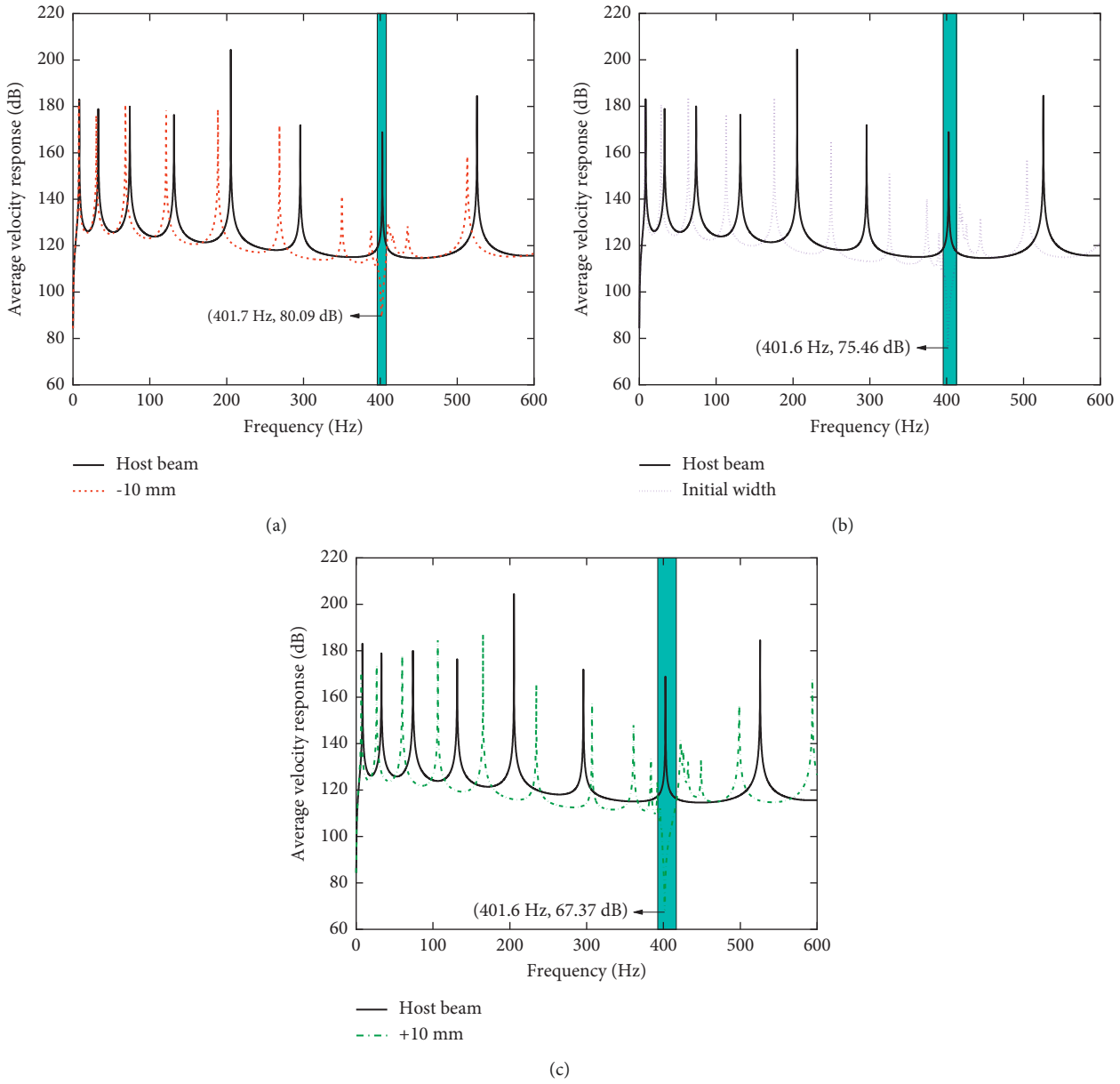

Figure 10: Influence of the beam-like resonator's width on the vibration properties of the locally resonant beam.

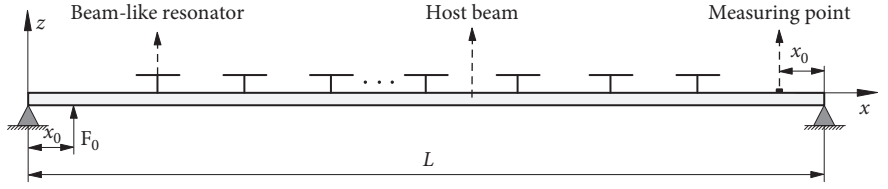

Figure 11: The analysis diagram concerns the vibration transmissibility of the finite locally resonant beam.

attenuation in the finite locally resonant beam is closer to the boundary of the bandgap, which can enhance the average vibration attenuation. Then, when the periodic number of units is large enough, the range of vibration attenuation completely matches the boundary of the bandgap, so the average vibration attenuation tends to be stable.

3.3. Determination of the Minimum Number of Units to Generate Bandgaps. The minimum number of units that can form a bandgap is studied in this section. The index used to evaluate the bandgap is as follows: the minimum average velocity response at the bandgap is lower than the 115.46 dB proposed in Section 3.2 by more than 20 dB. Two types of

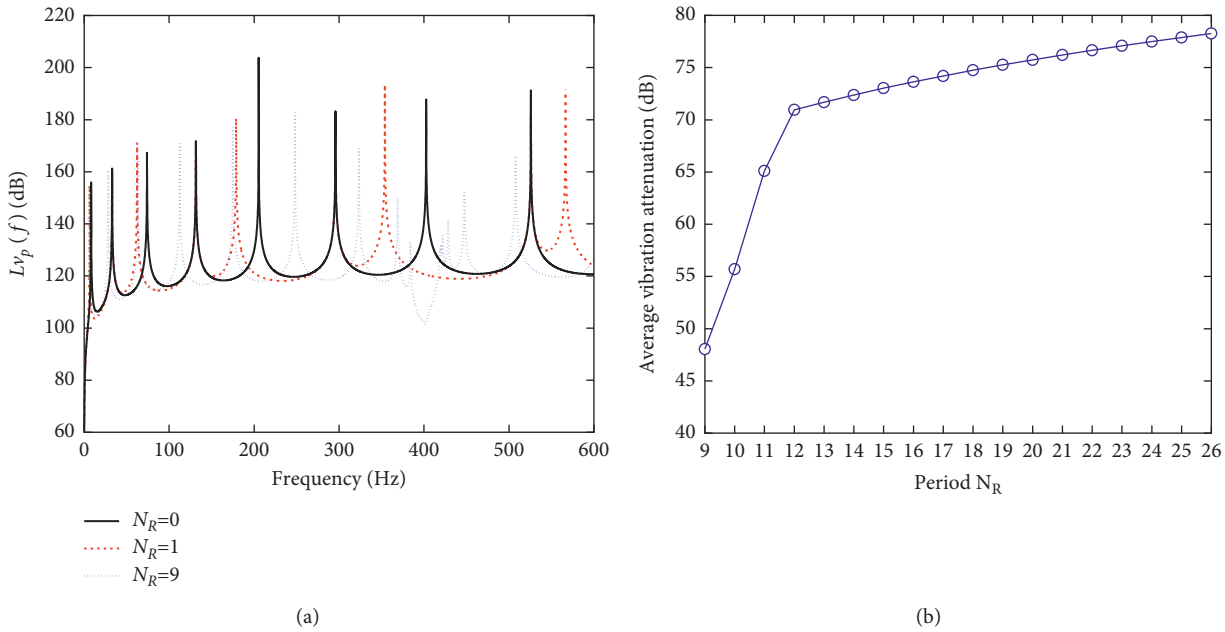

Figure 12: (a) The velocity response of the finite beam with different periods of units. (b) Effects of the period number of units on the average vibration attenuation within the bandgap.

Table 3: Parameters and resonance frequency of beam-like resonators.

	$2l$ (mm)	h (mm)	w (mm)	m (g)	f_r (Hz)
Resonator3	140	2	20	44.4	291.40
Resonator4	120	1.8	20	34.3	361.42

beam-like resonators are shown in Table 3, where the parameters are consistent with Table 2. We considered four types of locally resonant beams with different units: (i) the beam with several single-resonator units ($N = 1$) that contained Resonator2 (see Table 2). (ii) The beam with several double-resonator units ($N = 2$) that contained Resonator1 (see Table 2) and Resonator2. (iii) The beam with several three-resonator units ($N = 3$) that contained Resonator1, Resonator2, and Resonator3 (see Table 3). (iv) The beam with several four-resonator units ($N = 4$) that contained Resonator1, Resonator2, Resonator3, and Resonator4 (see Table 2). The average velocity responses of these beams with different types of units are shown in Figure 13.

We calculated the average velocity responses of the locally resonant beams with four types of units with the equations in Section 2.2, and the numerical results showed that the minimum number of units that can form bandgaps were all 10 ($M = 10$), based on the above-given index. The finite locally resonant beam with periodic arrays of multiple-resonator units could generate multiple bandgaps that corresponded to each resonator in a unit. Because of the coupling effect with each resonator in a unit, the vibration attenuation performance in the same bandgap is different, as shown in Figures 13(a)–13(d). In addition, it can be seen from Figure 13 that the resonance frequency of the finite locally resonant beam decreases with a greater total number (MN) of resonators. Meanwhile, multiple adjacent bandgaps can broaden the bandgap frequency range to achieve effective control of the vibration response with excitation at multiple frequencies. Determination of the minimum number of units to generate a bandgap for a locally resonant beam with different units is meaningful because it can reduce the design cost.

4. Experimental Results

To further validate the bandgap characteristics of the finite locally resonant beam, we built and tested an experimental sample of the finite locally resonant beam, which consisted of a simply supported beam and 12 periodically distributed beam-like resonators. The geometric parameters of the simply supported beam were as follows: length $L = 1.16$ m, width $B = 0.05$ m, and thickness $H = 0.005$ m. With regard to the material parameters, the beam had Young's modulus of $E = 6.8 \times 10^{10}$ Pa, Poisson's ratio of $\nu = 0.33$, and density of $\rho = 2860$ kg/m^3. The beam-like resonator was made of alloy steel with a material density $\rho_r = 7930$ kg/m^3, Young's modulus $E = 1.34 \times 10^{11}$ Pa, and Poisson's ratio $\nu_r = 0.3$, and the size of the beam-like resonator and its equivalent parameters are shown in Table 2, where $2l$, l_r, w, and t represent the total length, cantilever length, width, and thickness of the beam-like resonator, respectively, and m_0, m_r, k_r, and f_r represent the additional lumped mass, the effective mass, effective stiffness, and resonance frequency of the equivalent system, respectively. Each resonator was fixed on the simply supported beam by a shim with a width of 5 mm. The distance between adjacent resonators in the sample was $a = 90$ mm, and the distance between the installation position of the first and last resonators in the sample was 85 mm from the end of the simply supported beam.

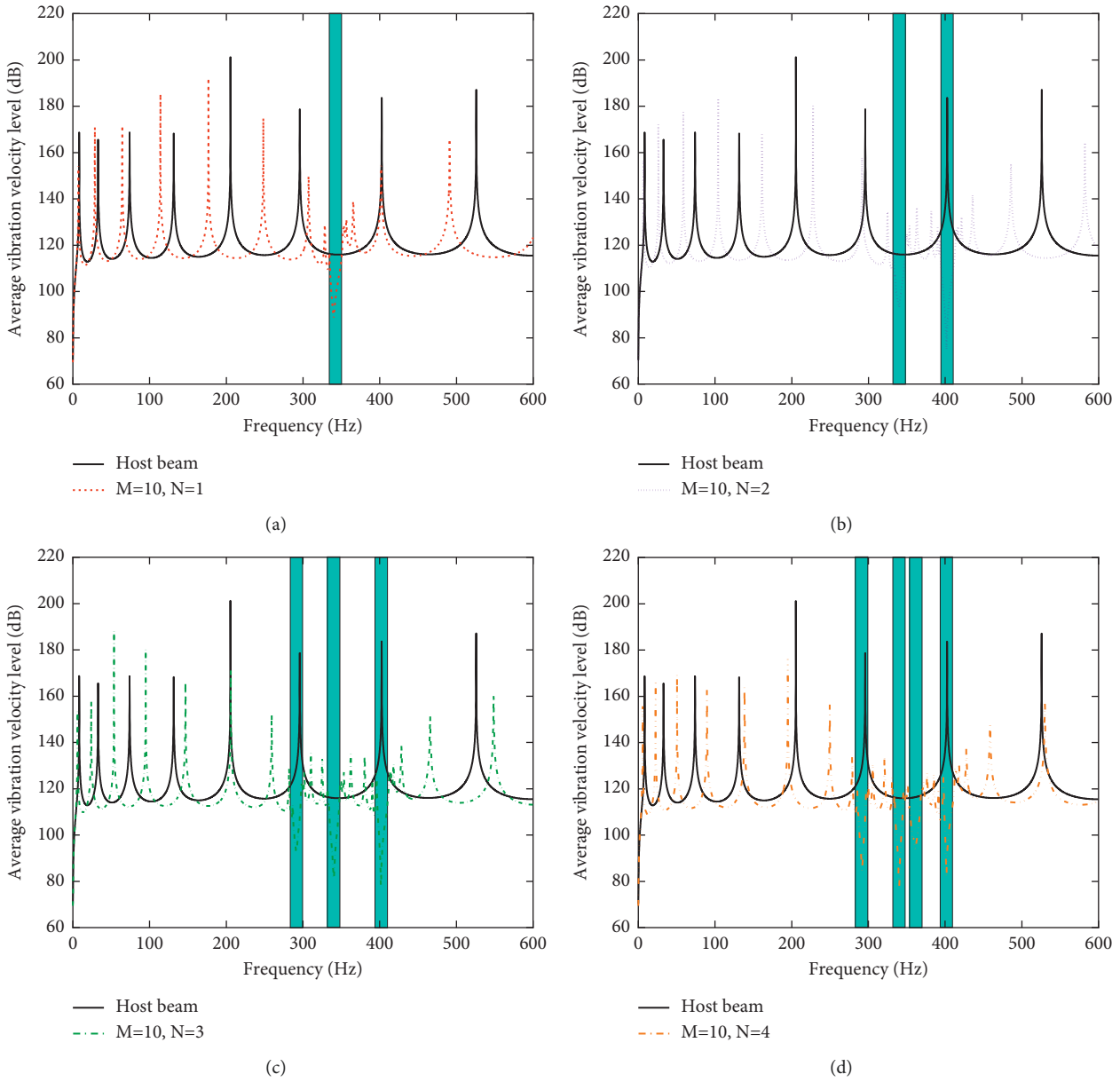

Figure 13: The average velocity response of the finite locally resonant beam with a minimum number of different types of units.

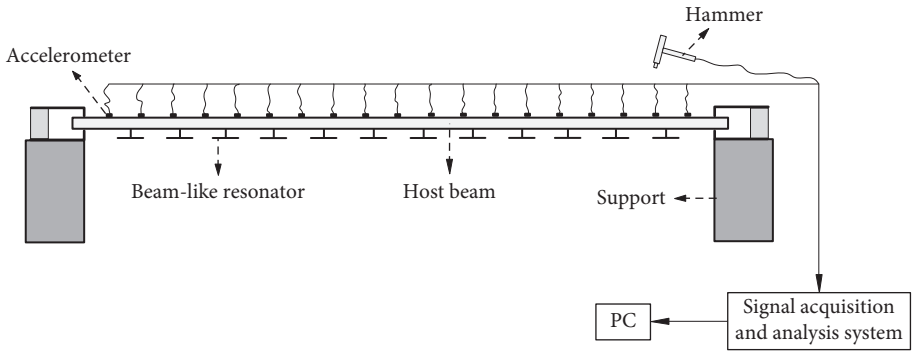

Figure 14: Schematic diagram of experimental system connection.

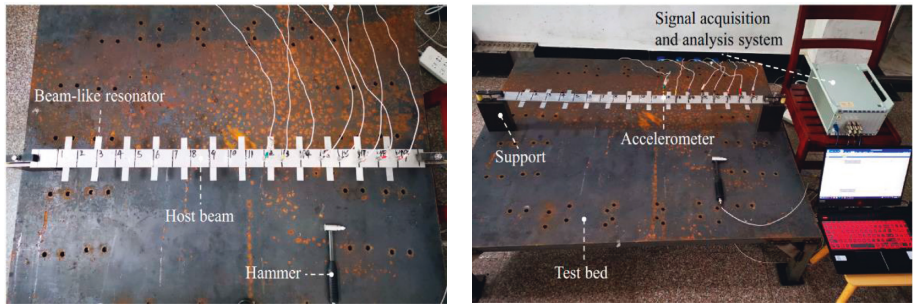

(a) (b)

Figure 15: (a) Locally resonant beam with 12 beam-like resonators and (b) experimental environment.

Table 4: Size and equivalent parameters of the beam-like resonator in experiment.

$2l$ (mm)	l_r (mm)	w (mm)	t (mm)	m_0 (g)	m_r (g)	k_r (N·m^{-1})	f_r (Hz)
126	121	20	2	18.4	25.5	1.61×10^5	399.01

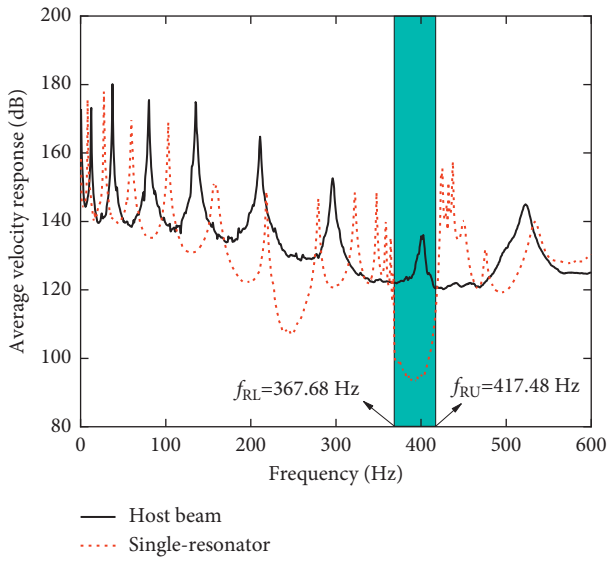

Figure 16: Average velocity responses of the simply supported beam without resonator and the locally resonant beam.

Figure 14 shows the schematic diagram of the experimental system connection. The primary equipment used in the experimental test was the DH5922D dynamic signal acquisition and analysis system. To simulate simply supported boundary conditions, the finite locally resonant beam was fixed in the test bed by two supports. Twelve beam-like resonators were evenly arranged onto one side of the finite beam, and ICP accelerometers were arranged at 20 measuring points on the other side of the beam. We applied an exciting force at the finite beam with a hammer. The experimental sample and experimental environment are shown in Figure 15. The signals measured by the hammer and accelerometer were processed by the signal acquisition and analysis system and then transferred to the computer for postprocessing, and the transfer functions measured by the 19 accelerations were averaged.

We processed the test data with (28) to obtain the average velocity response of the finite locally resonant beam under 1N excitation force; the measured results of the finite beam without resonators and the finite locally resonant beam with 12 beam-like resonators (see Table 4) are plotted in Figure 16.

$$L\overline{v}(\omega) = \sqrt{\frac{\sum_{i=1}^{N_m} \left[a_i(\omega)\omega/F(\omega)\right]^2}{N_m}}, \tag{28}$$

Figure 16 shows the average velocity response of the finite beam without a resonator and the finite locally resonant beam with periodic resonators. According to the bandgap calculation method explained in Section 3.2, the frequency range of the bandgap in the experiment was obtained as 367.68 Hz–417.48 Hz, which corresponded to the resonance frequency of the resonator, 399.01 Hz. The total mass of the beam-like resonators was 0.40 kg, which accounted for about 48.23% of the mass of the simply supported beam (0.8294 kg). This arrangement achieved vibration attenuation of the finite locally resonant beam at the bandgap by about 34.95 dB. Meanwhile, the resonance frequency of the finite beam decreased when periodic arrays of beam-like resonators were attached to the finite beam. Despite the expected difference, the measured results and theoretical analysis results were still in agreement. Therefore, we were able to realize a low-frequency vibration control method with a small, lightweight locally resonant beam.

5. Conclusion

In this paper, we designed a finite locally resonant beam with periodic arrays of beam-like resonators and studied the transverse vibration of the finite locally resonant beam theoretically by the modal superposition method and harmonic balance method, as well as experimentally. First, we arranged several periodic single-resonator units onto the finite beam and evaluated the performance in the bandgap of the beam. Then, we analyzed the influence of the length, thickness, width, and the number of resonators on the vibration characteristics of the finite locally resonant beam. We simulated the model of the finite locally resonant beam

with the finite element method to explore the effects of resonators on the vibration performance of the beam. Finally, the minimum number of locally resonant units that could generate bandgaps in the finite beam was obtained. Looking at the combined results from the theoretical analysis and experiments, the conclusions are as follows:

(i) The finite locally resonant beam can generate several low-frequency locally resonant bandgaps in the target frequency range, which is similar to the locally resonant beam with infinite boundary conditions.

(ii) The position, width, and vibration attenuation performance of bandgaps are influenced by the parameters and the periodic number of resonators. The position of bandgaps corresponds to the resonance frequency of each resonator. Increasing the length, thickness, and width of resonators can enhance vibration attenuation performance and widen the bandgap by the additional mass, which also affects the resonance frequency of the beam. As the number of resonators increases, the average vibration attenuation of the bandgap increases and tends to stabilize.

(iii) Multiresonators units have multiple bandgaps corresponding to the resonance frequency of each resonator in the unit. The minimum number of units that can generate bandgaps which reach the index is almost the same in the locally resonant beam with a different types of periodic units.

Data Availability

The data that support the findings of this study are available within the article.

Conflicts of Interest

The authors declare that there are no conflicts of interest.

Acknowledgments

This work was financially supported by the National Natural Science Foundation of China (Grant No. 11602300).

References

[1] H. H. Huang, C. T. Sun, and G. L. Huang, "On the negative effective mass density in acoustic metamaterials," *International Journal of Engineering Science*, vol. 47, no. 4, pp. 610–617, 2009.

[2] Y. Wu, Y. Lai, and Z. Q. Zhang, "Elastic metamaterials with simultaneously negative effective shear modulus and mass density," *Physical Review Letters*, vol. 107, no. 10, Article ID 105506, 2011.

[3] Z. Liu, X. Zhang, Y. Mao et al., "Locally resonant sonic materials," *Science*, vol. 289, no. 5485, pp. 1734–1736, 2000.

[4] D. Yu, Y. Liu, H. Zhao, G. Wang, and J. Qiu, "Flexural vibration band gaps in Euler-Bernoulli beams with locally resonant structures with two degrees of freedom," *Physical Review B*, vol. 73, no. 6, Article ID 064301, 2006.

[5] Y. Liu, D. Yu, L. Li, H. Zhao, J. Wen, and X. Wen, "Design guidelines for flexural wave attenuation of slender beams with local resonators," *Physics Letters A*, vol. 362, no. 5-6, pp. 344–347, 2007.

[6] C. Sugino, S. Leadenham, M. Ruzzene, and A. Erturk, "On the mechanism of bandgap formation in locally resonant finite elastic metamaterials," *Journal of Applied Physics*, vol. 120, no. 13, Article ID 134501, 2016.

[7] C. Sugino, Y. Xia, S. Leadenham, M. Ruzzene, and A. Erturk, "A general theory for bandgap estimation in locally resonant metastructures," *Journal of Sound and Vibration*, vol. 406, pp. 104–123, 2017.

[8] Y. Xiao, J. Wen, and X. Wen, "Flexural wave band gaps in locally resonant thin plates with periodically attached spring–mass resonators," *Journal of Physics D Applied Physics*, vol. 45, no. 19, Article ID 195412, 2012.

[9] E. M. Jr and J. Dos Santos, "Flexural wave band gaps in multi-resonator elastic metamaterial Timoshenko beams," *Wave Motion*, vol. 91, Article ID 102391, 2019.

[10] D. Beli, J. Arruda, and M. Ruzzene, "Wave propagation in elastic metamaterial beams and plates with interconnected resonators," *International Journal of Solids and Structures*, vol. 139-140, pp. 105–120, 2018.

[11] H. Lv, S. Li, X. Huang, and Z. Yu, "Band-gap properties of finite locally resonant beam suspended periodically with two-degree-of-freedom force type resonators," *Crystals*, vol. 11, no. 6, p. 716, 2021.

[12] G. Failla, R. Santoro, A. Burlon, and A. F. Russillo, "An exact approach to the dynamics of locally-resonant beams," *Mechanics Research Communications*, vol. 103, Article ID 103460, 2020.

[13] A. F. Russillo, G. Failla, and F. Fraternali, "Free and forced vibrations of damped locally-resonant sandwich beams," *European Journal of Mechanics - A: Solids*, vol. 86, Article ID 104188, 2021.

[14] L. Sangiuliano, C. Claeys, E. Deckers, and W. Desmet, "Influence of boundary conditions on the stop band effect in finite locally resonant metamaterial beams," *Journal of Sound and Vibration*, vol. 473, Article ID 115225, 2020.

[15] D. J. Thompson, "A continuous damped vibration absorber to reduce broad-band wave propagation in beams," *Journal of Sound and Vibration*, vol. 311, no. 3-5, pp. 824–842, 2008.

[16] R. Chen and T. Wu, "Vibration control of base system using distributed dynamic vibration absorbers," *Journal of Vibration and Control*, vol. 20, no. 10, pp. 1589–1600, 2014.

[17] M. Y. Wang, Y. T. Choy, and C. W. Wan, A. S. Zhao, Wide Band-Gaps in flexural periodic beams with separated force and moment resonators," *Journal of Vibration and Acoustics*, vol. 137, no. 6, 2015.

[18] J. Zhou, K. Wang, D. Xu, and H. Ouyang, "Local resonator with high-static-low-dynamic stiffness for lowering band gaps of flexural wave in beams," *Journal of Applied Physics*, vol. 121, no. 4, Article ID 044902, 2017.

[19] C. Claeys, N. G. S. M. F. Rocha, L. V. Belle, E. Deckers, and W. Desmet, "Design and validation of metamaterials for multiple structural stop bands in waveguides," *Extreme Mechanics Letters*, vol. 12, pp. 7–22, 2017.

[20] G. Habib, T. Detroux, R. Viguié, and G. Kerschen, "Nonlinear generalization of Den Hartog's equal-peak method," *Mechanical Systems and Signal Processing*, vol. 52-53, no. 1, pp. 17–28, 2015.

[21] A. Casalotti and W. Lacarbonara, "Tailoring of pinched hysteresis for nonlinear vibration absorption via asymptotic

analysis," *International Journal of Non-linear Mechanics*, vol. 94, pp. 59–71, 2017.

[22] A. Casalotti, S. El-Borgi, and W. Lacarbonara, "Metamaterial beam with embedded nonlinear vibration absorbers," *International Journal of Non-linear Mechanics*, vol. 98, pp. 32–42, 2018.

[23] H. M. El-Khatib, B. R. Mace, and M. J. Brennan, "Suppression of bending waves in a beam using a tuned vibration absorber," *Journal of Sound and Vibration*, vol. 288, no. 4-5, pp. 1157–1175, 2005.

[24] Y. Xiao, J. H. Wen, G. Wang, and X. Wen, "Theoretical and experimental study of locally resonant and Bragg band gaps in flexural beams carrying periodic arrays of beam-like resonators," *Journal of Vibration and Acoustics*, vol. 135, no. 4, Article ID 041006, 2013.

[25] J. O. Vasseur, P. A. Deymier, B. Chenni, B. Djafari-Rouhani, L. Dobrzynski, and D. Prevost, "Experimental and theoretical evidence for the existence of absolute acoustic band gaps in two-dimensional solid phononic crystals," *Physical Review Letters*, vol. 86, no. 14, pp. 3012–3015, 2001.

[26] F. Wu, Z. Hou, Z. Liu, and Y. Liu, "Acoustic band gaps in two-dimensional rectangular arrays of liquid cylinders," *Solid State Communications*, vol. 123, no. 5, pp. 239–242, 2002.